



Microwave Observations of Venus with CLASS

Sumit Dahal^{1,2}, Michael K. Brewer², Alex B. Akins³, John W. Appel², Charles L. Bennett², Ricardo Bustos⁴, Joseph Cleary², Jullianna D. Couto², Rahul Datta², Joseph Eimer², Thomas Essinger-Hileman^{1,2}, Jeffrey Iuliano^{2,5}, Yunyang Li (李云扬)², Tobias A. Marriage², Carolina Núñez², Matthew A. Petroff^{2,6}, Rodrigo Reeves⁷, Karwan Rostem¹, Rui Shi (时瑞)², Deniz A. N. Valle², Duncan J. Watts^{2,8}, Janet L. Weiland², Edward J. Wollack¹, and Zhilei Xu (徐智磊)^{2,9}

¹ NASA Goddard Space Flight Center, 8800 Greenbelt Road, Greenbelt, MD 20771, USA; sumit.dahal@nasa.gov

² The William H. Miller III Department of Physics and Astronomy, Johns Hopkins University, 3701 San Martin Drive, Baltimore, MD 21218, USA

³ Jet Propulsion Laboratory, California Institute of Technology, Instruments Division, Pasadena, CA 91011, USA

⁴ Facultad de Ingeniería, Universidad Católica de la Santísima Concepción, Alonso de Ribera 2850, Concepción, Chile

⁵ Department of Physics and Astronomy, University of Pennsylvania, 209 South 33rd Street, Philadelphia, PA 19104, USA

⁶ Center for Astrophysics, Harvard & Smithsonian, 60 Garden Street, Cambridge, MA 02138, USA

⁷ CePIA, Departamento de Astronomía, Universidad de Concepción, Concepción, Chile

⁸ Institute of Theoretical Astrophysics, University of Oslo, P.O. Box 1029 Blindern, NO-0315 Oslo, Norway

⁹ MIT Kavli Institute, Massachusetts Institute of Technology, 77 Massachusetts Avenue, Cambridge, MA 02139, USA

Received 2023 April 14; revised 2023 August 5; accepted 2023 August 7; published 2023 August 29

Abstract

We report on the disk-averaged absolute brightness temperatures of Venus measured at four microwave frequency bands with the Cosmology Large Angular Scale Surveyor. We measure temperatures of 432.3 ± 2.8 , 355.6 ± 1.3 , 317.9 ± 1.7 , and 294.7 ± 1.9 K for frequency bands centered at 38.8, 93.7, 147.9, and 217.5 GHz, respectively. We do not observe any dependence of the measured brightness temperatures on solar illumination for all four frequency bands. A joint analysis of our measurements with lower-frequency Very Large Array observations suggests relatively warmer (~ 7 K higher) mean atmospheric temperatures and lower abundances of microwave continuum absorbers than those inferred from prior radio occultation measurements.

Unified Astronomy Thesaurus concepts: Venus (1763); Brightness temperature (182); Atmospheric composition (2120)

1. Introduction

Since the late 1950s, several spacecraft and Earth-based observatories have probed the Venusian surface and atmosphere at various radio wavelengths (Mayer et al. 1958; Barrett & Staelin 1964; Pollack & Sagan 1967; de Pater 1990; Pettengill et al. 1992; Butler et al. 2001). These observations have established that Venus has a hot surface (~ 750 K) surrounded by a very thick atmosphere primarily consisting of CO_2 ($\sim 96\%$) with a small amount of N_2 and trace amounts of other molecules like SO_2 and H_2SO_4 (Muhleman et al. 1979; Oyama et al. 1979). While radio wavelengths longer than a few centimeters probe the hot Venusian surface, decreasing wavelengths successively probe increasing altitudes in the atmosphere (Butler et al. 2001; Akins 2020). The atmospheric gases and aerosols provide significant microwave opacity, resulting in a steep temperature decrease in the spectrum at shorter wavelengths. An accurate measurement of the Venus microwave brightness temperature spectrum can therefore provide valuable information about the composition and dynamics of various layers of its atmosphere. In this paper, we report on the disk-averaged brightness temperatures of Venus at four microwave bands, measured with the Cosmology Large Angular Scale Surveyor (CLASS; Essinger-Hileman et al. 2014; Harrington et al. 2016).

CLASS is an array of microwave polarimeters that surveys 75% of the sky every day from the Atacama Desert at four

frequency bands centered near 40, 90, 150, and 220 GHz. All CLASS telescopes use feedhorn-coupled transition-edge sensor bolometers cooled to temperatures of $\lesssim 60$ mK to make high-sensitivity measurements (Dahal et al. 2022) of microwave sources on the sky. This paper is a follow-up to Dahal et al. (2021), where the most precise Venus brightness temperature measurements to date in the Q and W frequency bands centered near 40 and 90 GHz, respectively, were presented. Since then, a dichroic G -band (150/220 GHz) instrument (Dahal et al. 2020) has been added to CLASS. We describe the Venus observations performed with the CLASS G -band instrument in Section 2. In Section 3, we present the results from our brightness temperature measurements and examine the phase dependence of the measured temperatures. In Section 4, we discuss Venus atmospheric modeling. Section 5 presents an empirically perturbed model that is consistent with our observations. Finally, we provide a summary in Section 6.

2. CLASS Observations

CLASS is designed to make precise measurements of the cosmic microwave background (CMB) polarization on large angular scales. During the nominal survey mode, CLASS scans the microwave sky azimuthally at 45° elevation from a site located at $22^\circ 58' \text{S}$ latitude and $67^\circ 47' \text{W}$ longitude with an altitude of approximately 5200 m. Periodically, CLASS performs dedicated observations of bright sources—the Moon, Venus, and Jupiter—to calibrate the detector response, obtain telescope pointing information, and characterize the instrument beam (Xu et al. 2020; Datta et al. 2022). During the dedicated Moon/planet observations, the telescopes scan across the



Original content from this work may be used under the terms of the [Creative Commons Attribution 4.0 licence](https://creativecommons.org/licenses/by/4.0/). Any further distribution of this work must maintain attribution to the author(s) and the title of the work, journal citation and DOI.

source in azimuth at a fixed elevation as the source rises or sets through the telescopes' fields of view. In Dahal et al. (2021), we used the dedicated planet observations to obtain the brightness temperatures of Venus at the Q and W bands, using Jupiter as a calibration source. Following the same procedure, we extend our brightness temperature measurements to two higher CLASS frequency bands centered near 150 and 220 GHz in this paper.

Between 2021 November 13 and 2022 February 24, the CLASS dichroic G -band telescope performed 65 dedicated Venus scans. The same G -band instrument configuration observed Jupiter 59 times between 2022 September 26 and 2022 November 7. For each of these observations, we combine the acquired time-ordered data (TOD) with the telescope pointing information to generate planet-centered maps for each detector on the focal plane. The raw detector TOD is calibrated to the measured optical power through detector current versus voltage (I - V) measurements acquired prior to each observation. We use a robust binned I - V calibration method described in Appel et al. (2022) with a 1% median error in per-detector calibration across all observations.

For each of the planet-centered maps, the measured optical power is corrected for atmospheric transmission to account for the effect of precipitable water vapor (PWV) at the CLASS site (Pardo et al. 2001). We use the detector optical loading obtained from I - V measurements to estimate the PWV at the CLASS site. The relationship between the PWV and the detector optical loading is described in Appel et al. (2022). We verify that the derived brightness temperatures (Section 3.2) show no dependence on PWV within the measurement uncertainties, increasing our confidence in the atmospheric opacity correction.

Since the angular diameters ($\lesssim 1'$) for both Venus and Jupiter are much smaller than the telescope beam sizes (FWHM of $23'$ for 150 GHz and $16'$ for 220 GHz), the planets can be approximated as point sources for CLASS telescopes. Therefore, following Page et al. (2003), the brightness temperature of the planet T_p can be calculated as

$$T_p = T_m \times (\Omega_B / \Omega_p), \quad (1)$$

where Ω_p is the solid angle subtended by the planet, Ω_B is the telescope beam solid angle, and T_m is the measured peak detector response (amplitude of an elliptical Gaussian fit to the data) from the planet-centered maps after correcting for the atmospheric transmission during the observations. Refer to Xu et al. (2020) and Datta et al. (2022) for further details on the data acquisition and mapmaking used to obtain T_m from dedicated CLASS observations.

3. Results

During the observing campaign, 390 detectors for 150 GHz and 209 detectors for 220 GHz detected both planets at least 20 times. We analyze these observations in two different ways: (1) per-detector averaging of the respective planet observations to constrain the Venus brightness temperature (Section 3.1) and (2) per-observation averaging of the respective detector arrays to examine the phase dependence of the measured temperatures (Section 3.2).

3.1. Brightness Temperature

For every operating detector on the G -band focal plane, we obtain an aggregate planet-centered map by averaging individual maps relative to a fiducial solid angle Ω_{ref} . This is performed by scaling the PWV-corrected detector response T_m by a factor of $\Omega_{\text{ref}}/\Omega_p$ while averaging. Since the choice of Ω_{ref} does not affect our final results (see Equation (2)), we arbitrarily set $\Omega_{\text{ref}} = 3.8 \times 10^{-8}$ sr (i.e., $45''45$ angular diameter) for averaging the maps. For a given observation, Ω_p is determined using the distance to the planet with a fixed disk radius R . As discussed in Dahal et al. (2021), we use $R = 6120$ km for Venus and $R = 69,140$ km for Jupiter. The latter is an “effective R ” for the projected area of Jupiter’s oblate disk (Weiland et al. 2011) calculated using the average Jupiter sub-Earth latitude of $2^\circ.81$ during the observing campaign.

Since both the Venus and Jupiter maps are averaged relative to the same Ω_{ref} , the ratio of their brightness temperatures (Equation (1)) for a given detector reduces to

$$\frac{T_{p=\text{Ven}}}{T_{p=\text{Jup}}} = \frac{T_m^{\text{Ven,ref}} \times (\Omega_B / \Omega_{\text{ref}})}{T_m^{\text{Jup,ref}} \times (\Omega_B / \Omega_{\text{ref}})} = \frac{T_m^{\text{Ven,ref}}}{T_m^{\text{Jup,ref}}}. \quad (2)$$

Equation (2) shows that the brightness temperature ratio is simply the ratio of the measured peak responses when scaled to the same Ω_{ref} and does not depend on individual detector properties like Ω_B . For simplicity, we will refer to the individual planet brightness temperatures $T_{p=\text{Ven}}$ and $T_{p=\text{Jup}}$ as T_{Ven} and T_{Jup} , respectively.

Figure 1 shows the $T_{\text{Ven}}/T_{\text{Jup}}$ ratios derived from 387 detectors for 150 GHz and 204 detectors for 220 GHz in the CLASS G -band instrument. The uncertainties in the ratios are the combined errors obtained from the variance of baseline measurements away from the source for both the Venus and Jupiter maps. For this analysis, we discarded three outliers (out of 390) for 150 GHz and five (out of 209) for 220 GHz with ratios outside three standard deviations from the mean of their respective distributions. For the distributions shown in Figure 1, the inverse-variance weighted mean ratios are 1.822 ± 0.002 and 1.675 ± 0.003 for 150 and 220 GHz, respectively, where the uncertainties are the standard errors on the mean. To verify that these errors represent the uncertainties in the mean of the underlying distribution, we use bootstrapping to generate 10^6 resamples. For both 150 and 220 GHz, the standard deviation of the mean values of the bootstrapped resamples is the same as the standard error calculated from the parent distribution shown in Figure 1.

To obtain T_{Ven} , we multiply the mean CLASS-measured $T_{\text{Ven}}/T_{\text{Jup}}$ ratios by the corresponding T_{Jup} values measured by the Planck satellite (Planck Collaboration Int. LII 2017). For the higher CLASS G band with an effective Rayleigh–Jeans (RJ) point-source center frequency of 217.5 ± 1.0 GHz (Dahal et al. 2022), we use $T_{\text{Jup}} = 175.8 \pm 1.1$ K from the Planck 217 GHz measurement. For the lower G band with an effective center frequency of 147.9 ± 1.0 GHz, we use $T_{\text{Jup}} = 174.2 \pm 0.9$ K, which is 0.1 K higher than the Planck measurement at 143 GHz. This 0.1 K correction takes into account the difference between the CLASS and Planck center frequencies and is obtained through a local power-law fit between the two Planck T_{Jup} values at 143 and 217 GHz. Given a relatively flat T_{Jup} spectrum at the G band, we obtain the same correction when extrapolating a power-law fit from Planck

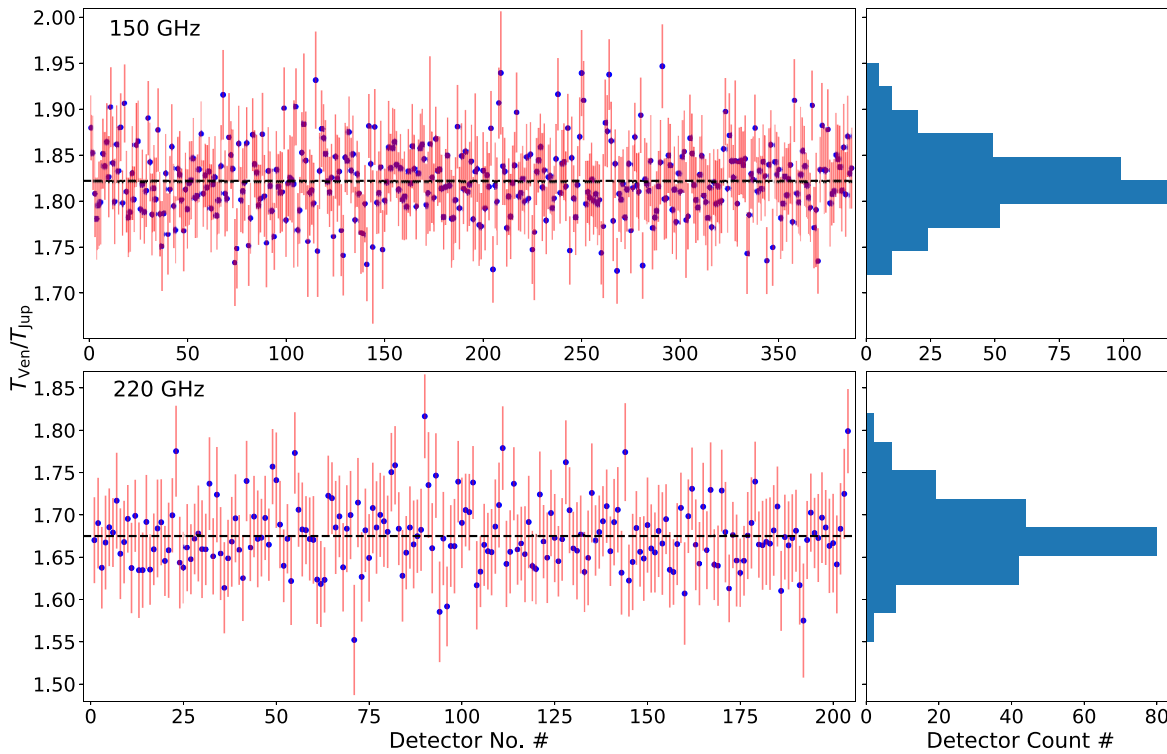


Figure 1. The $T_{\text{Ven}}/T_{\text{Jup}}$ ratio measurements (left) and the corresponding histograms (right) from the CLASS dichroic G -band instrument. The uncertainties (red bars) in the measured ratios (blue dots) are the combined errors obtained from the variance of baseline measurements away from the planets. The inverse-variance weighted mean ratios (dashed lines) are 1.822 ± 0.002 and 1.675 ± 0.003 for 150 and 220 GHz, respectively, where the uncertainties are the standard errors on the mean.

100 and 143 GHz measurements as well. The nominal RadiobEAR model¹⁰ yields a slightly higher correction of 0.17 K, but we find this to be less reliable, as the model spectrum is $\sim 2\text{--}3$ K higher than the Planck measurements in this frequency range. While both corrections are well within the T_{Jup} uncertainty, we adopt the local power law–obtained correction for further analysis, as it is consistent across multifrequency Planck measurements.

Using these T_{Jup} values and the mean CLASS-measured $T_{\text{Ven}}/T_{\text{Jup}}$ ratios shown in Figure 1, we obtain T_{Ven} of 317.3 ± 1.7 and 294.5 ± 1.9 K for frequency bands centered at 147.9 ± 1.0 and 217.5 ± 1.0 GHz, respectively. These T_{Ven} values represent the disk-averaged Venus brightness temperatures measured with respect to blank sky. The absolute brightness temperatures can be obtained by adding the RJ temperatures of the CMB (0.6 K at 147.9 GHz and 0.2 K at 217.5 GHz), resulting in 317.9 ± 1.7 and 294.7 ± 1.9 K, respectively. Table 1 summarizes the CLASS measurements of the Venus brightness temperatures at four microwave frequency bands, including the measurements at two lower bands presented in Dahal et al. (2021). It is worth noting that the T_{Jup} values in Table 1 used to calibrate our T_{Ven} measurements are mean disk-integrated brightness temperatures obtained from multiyear Wilkinson Microwave Anisotropy Probe (WMAP)/Planck observations. While temporal temperature variabilities have been reported for different Jovian latitude bands (Orton et al. 2023), the disk-averaged temperatures at the frequency bands presented here were found to be stable within the reported uncertainties over 9 yr of WMAP (Bennett et al. 2013) and 4 yr of Planck (Planck Collaboration Int. LII 2017) observing seasons.

¹⁰ <https://github.com/david-deboer/radiobear>

Table 1
Summary of CLASS Measurements

ν_c^{RJ} (GHz) ^a	$T_{\text{Ven}}/T_{\text{Jup}}$	T_{Jup} (K)	T_{Ven} (K) ^b
38.8 ± 0.5	2.821 ± 0.015	$152.6 \pm 0.6^{\text{c}}$	430.4 ± 2.8
93.7 ± 0.8	2.051 ± 0.004	$172.8 \pm 0.5^{\text{c}}$	354.5 ± 1.3
147.9 ± 1.0	1.822 ± 0.002	$174.2 \pm 0.9^{\text{d}}$	317.3 ± 1.7
217.5 ± 1.0	1.675 ± 0.003	$175.8 \pm 1.1^{\text{d}}$	294.5 ± 1.9

Notes.

^a Effective RJ point-source center frequencies; see Dahal et al. (2022).

^b Temperature values with respect to blank sky. Absolute brightness temperatures can be obtained by adding the RJ temperatures of the CMB of 1.9, 1.1, 0.6, and 0.2 K at 38.8, 93.7, 147.9, and 217.5 GHz, respectively, calculated using the 2.725 K blackbody temperature of the CMB (Fixsen 2009).

^c Obtained from Bennett et al. (2013); includes 1.7 K correction for 38.8 GHz (see Dahal et al. 2021 for details).

^d Obtained from Planck Collaboration Int. LII (2017); includes 0.1 K correction for 147.9 GHz.

3.2. Phase

In Section 3.1, we averaged all of the individual planet observations, increasing the signal-to-noise ratio of the per-detector aggregate maps to better constrain the Venus brightness temperature. Here we calculate an array-averaged brightness temperature value for every dedicated Venus observation to examine the phase dependence of the measured temperatures. For a given detector, the denominator value in Equation (2) remains the same, but now we calculate the $T_{\text{Ven}}/T_{\text{Jup}}$ ratio and thus the T_{Ven} value separately for each Venus observation. Finally, we average the T_{Ven} values obtained from all detectors in the array for each observation.

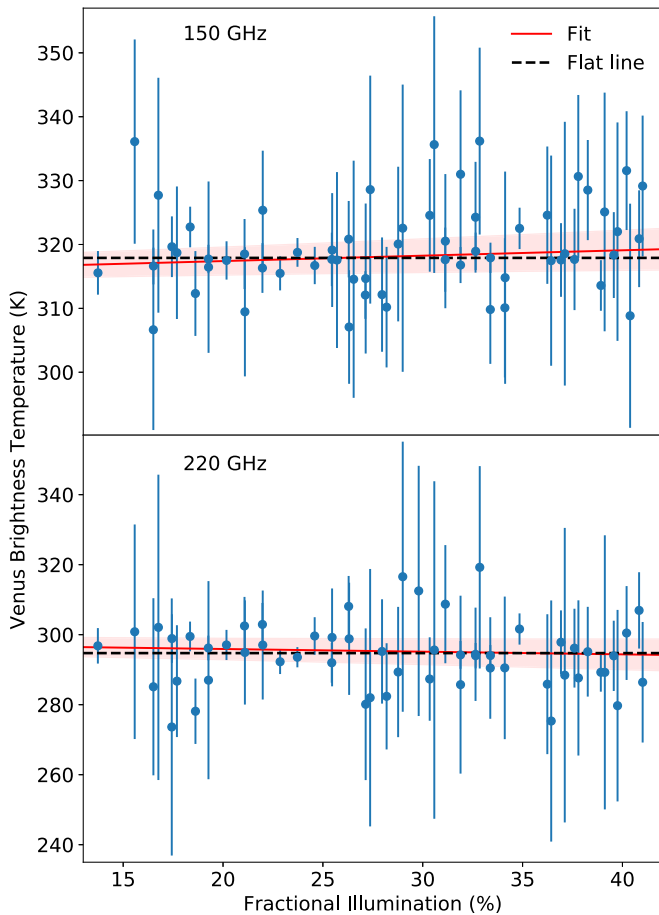


Figure 2. Measured array-averaged Venus brightness temperature vs. fractional solar illumination. The uncertainties on the data points are the standard errors on the mean. The flat lines (dashed black) centered at the absolute brightness temperature values from Table 1 fall within the 1σ uncertainty (red shading) of the linear best-fit lines (solid red). There is no statistically significant phase dependence of the measured temperatures at both frequency bands.

Figure 2 shows the array-averaged T_{Ven} versus fractional solar illumination (phase) of Venus during the observations. During the CLASS *G*-band observing campaign, the solar illumination of Venus varied from 13.7% to 41.0%. However, we do not see a statistically significant phase dependence of the observed brightness temperatures at either frequency band. The linear fit lines with gradients of 0.08 ± 0.07 K/% for 150 GHz and -0.08 ± 0.09 K/% for 220 GHz are statistically consistent with being flat. This result is consistent with the absence of phase variation observed at the two lower CLASS frequency bands (Dahal et al. 2021) and the range of phase-dependent temperature variations inferred from prior radio occultation measurements (Tellmann et al. 2009).

4. Atmospheric Modeling

The CLASS observations of the disk-averaged Venus brightness temperatures presented here are the most precise measurements to date at these frequency bands. Figure 3 and Table 2 show the CLASS measurements in context with other published microwave observations. Given that the wavelengths shorter than ~ 2 cm are primarily sensitive to Venusian atmospheric emission, precise microwave observations can be used to study the composition and dynamics of various layers of the Venusian atmosphere. Here we perform a joint analysis

of the CLASS observations from ~ 1 to 8 mm and the Very Large Array (VLA) measurements of Perley & Butler (2013) from ~ 7 mm to 2 cm to obtain constraints on the accuracy of the Venus atmospheric composition models.

Despite the precision of the CLASS and VLA brightness temperature measurements, fitting to the disk-averaged spectrum is broadly challenging due to the unresolved nature of the observations and the considerable latitudinal variation in the Venusian atmospheric structure and composition. In principle, it is possible to find an atmospheric model with arbitrary parameters that would produce an exact fit to the measured spectrum. However, the results obtained from such a fit with input parameters that are not physically motivated would not be particularly informative. Therefore, we start with a latitude-dependent atmospheric model informed by radio occultation measurements and other prior analyses and then scale the model parameters globally to obtain an empirically perturbed model that is consistent with the CLASS and VLA spectra.

We use a two-dimensional, zonally averaged, hemispherically symmetric atmospheric model with 250 m vertical and 5° latitude resolution. The temperature and pressure profiles for the model are taken from the original Venus International Reference Atmosphere (Seiff et al. 1985). Between the 40 and 90 km altitudes, the temperature profiles are merged with those determined by Ando et al. (2020) from radio occultation refractivity measurements with the Venus Express (VEX; Svedhem et al. 2007) and Akatsuki (Nakamura et al. 2016) space probes. The bulk atmospheric composition is 96.5% CO_2 and 3.5% N_2 , and trace species, including SO_2 gas and H_2SO_4 vapor and aerosol, are the primary continuum microwave absorbers. The abundance and spatial distribution of these trace species impact the observed brightness temperature spectrum. For our reference model, we use latitude-dependent SO_2 abundance and H_2SO_4 vapor profiles (Oschlisniok et al. 2021) based on the VEX radio absorption measurements. This SO_2 profile has a uniform abundance beneath 55 km with rapid depletion above that altitude and features subcloud abundances on the order of 50 ppm at lower latitudes, increasing to 150 ppm at the poles. The latitudinally varying H_2SO_4 vapor profile has maximal abundance values of ~ 12 ppm at equatorial and polar latitudes around 43–47 km altitude. The cloud aerosol mass profiles are taken from the atmospheric transport model of Oschlisniok et al. (2021), which reproduces the VEX H_2SO_4 vapor distribution well. For the range of aerosol particle sizes inferred from the Pioneer Venus cloud particle size spectrometer (LCPS; Knollenberg & Hunten 1980), we expect the effect from scattering to be negligible, as the scattering cross section for these aerosols is multiple orders of magnitude below their absorption cross section at CLASS frequencies (Fahd 1992; Akins 2020). While their impact on the brightness temperature spectrum is expected to be minimal, other species above 1 ppm abundance, specifically H_2O , CO , and OCS , are also included at their nominal abundances (Krasnopolsky 2007, 2012).

The model surface, which primarily affects the brightness temperatures at wavelengths $\gtrsim 2$ cm, is set to be uniform with a dielectric constant (ϵ_r) of 4 obtained from the average of the emissivity and reflectivity values determined from the Magellan radar/radiometer observations (Pettengill et al. 1992). Jenkins et al. (2002) followed the same approach for their analysis of spatially resolved VLA observations at wavelengths up to ~ 2 cm, further validating our surface

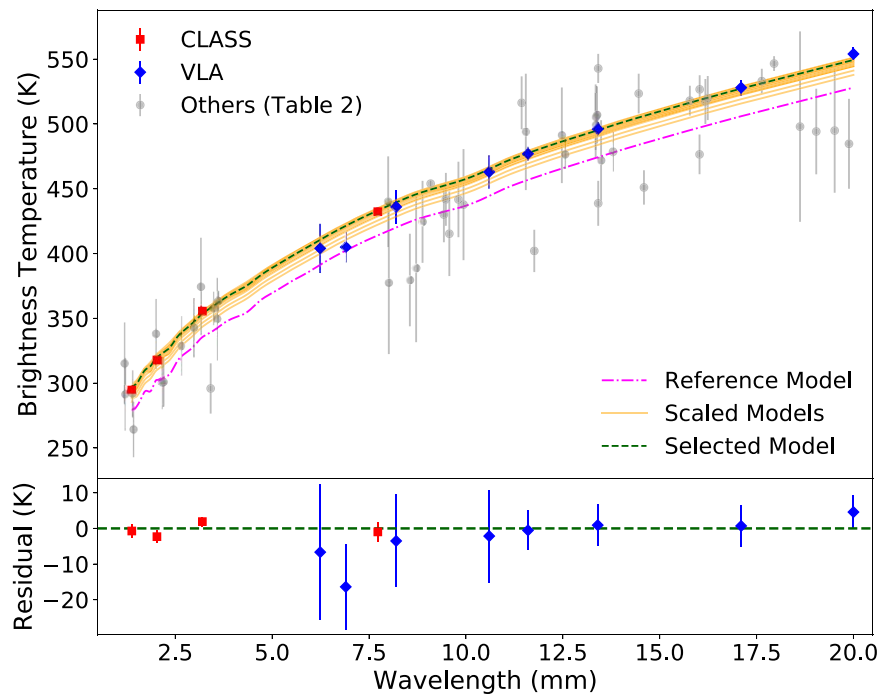


Figure 3. Disk-averaged Venus brightness temperature measurements at 1 mm–2 cm wavelengths. The data points, along with their references, are listed in Table 2. The magenta dashed–dotted curve is the reference Venusian atmospheric model determined from the radio occultation data, and the solid orange curves are obtained by scaling various model parameters (see Section 5 for details) from the reference model. The green dashed curve shows the scaled model that is most consistent with the CLASS and VLA measurements, which are among the most precise measurements to date in this wavelength range.

assumption for comparison to the disk-averaged CLASS observations at shorter wavelengths. At these wavelengths, the effect of Bragg and volume scattering by the Venusian surface is negligible. The radiative transfer calculations are equivalent to those described in detail by Butler et al. (2001) and Akins (2020). The atmosphere is assumed to be locally plane-parallel, and optical paths are determined via a ray-tracing approach, which accounts for Venus’s significant atmospheric refraction and incorporates limb-emission effects at the edge of the Venusian disk. The opacities within each homogeneous layer are computed with either continuum or line-by-line opacity models for CO_2/N_2 , SO_2 , H_2SO_4 aerosol, and H_2SO_4 vapor determined from laboratory measurements. We use the models from Fahn & Steffes (1991, 1992) and Akins & Steffes (2020) for SO_2 , H_2SO_4 aerosol, and H_2SO_4 vapor, respectively.

Figure 3 shows the brightness temperature spectrum obtained from the described model (magenta dashed–dotted curve). This nominal atmospheric model determined from the radio occultation data produces a spectrum that is colder than the CLASS and VLA measurements, similar to the results from Butler et al. (2001) and Jenkins et al. (2002). To obtain a model that is consistent with the CLASS and VLA measurements, we perturb the nominal reference model by uniformly scaling the abundances of the molecular absorbers (multiplicatively) and the temperature profiles (additively).

5. Discussion

At shorter millimeter wavelengths, the CLASS measurements are particularly important in constraining the models within the cloud region. For our reference model, however, we find that the shorter-wavelength CLASS measurements are even warmer than those predicted if the only sources of opacity

were CO_2 and N_2 . The only way to resolve this discrepancy within the context of the atmospheric model is to increase the magnitude of the physical temperature profile adopted to parameterize the observations in the model. Based on past analyses, it is also not realistic to completely remove SO_2 and H_2SO_4 from the Venusian atmosphere. Therefore, we examine several scaled models with different combinations of increased temperatures and decreased absorber abundances to find a model that is consistent with the CLASS and VLA measurements. For this paper, we explore 28 different models with (1) increases in mean temperature between 0 and 8 K; (2) total SO_2 , H_2SO_4 vapor, and H_2SO_4 aerosol abundances varied individually in the range between 0.6 and 1.0 times the nominal values described in Section 4 for the reference model; and (3) an additional cutoff altitude parameter varied between 50 and 60 km, above which the H_2SO_4 aerosol and SO_2 abundances were set to zero.

The brightness temperature spectra for the 28 scaled models considered in our analysis are shown in Figure 3. The green dashed curve shows the scaled model with the lowest χ^2 value (reduced χ^2 of ~ 1.1 for seven degrees of freedom). Compared to the reference model, this selected model was obtained by increasing the temperature profile by 7 K; decreasing the SO_2 , H_2SO_4 vapor, and H_2SO_4 aerosol abundances by 30%; and setting the cutoff altitude to ~ 55 km. While this empirically perturbed model produces a good fit to the CLASS and VLA brightness temperature measurements, we cannot rule out other models that have slightly warmer temperatures and higher absorber abundances, or vice versa.

Regardless of the particular choice of the best-fit model, all of our scaled models that produce a reasonable fit to the CLASS and VLA observations suggest a necessary depletion of microwave opacity within the Venusian middle cloud region. This result is consistent with other observational

Table 2
Disk-averaged Microwave Venus Brightness Temperature Measurements

Wavelength (mm)	T_{Ven} (K)	References	Wavelength (mm)	T_{Ven} (K)	References
1.19	315.3 ± 31.6	Muhleman et al. (1979)	9.94	437.8 ± 42.9	Muhleman et al. (1979)
1.22	291.3 ± 28.2	Ulich (1974)	10.6	463 ± 13	Perley & Butler (2013)
1.38	294.7 ± 1.9	This work	11.44	516.3 ± 20.4	Muhleman et al. (1979)
1.4	291.8 ± 18.4	Muhleman et al. (1979)	11.55	493.9 ± 44.9	Muhleman et al. (1979)
1.43	264.3 ± 21.4	Muhleman et al. (1979)	11.6	477 ± 5.5	Perley & Butler (2013)
2	338 ± 27	Fasano et al. (2021)	11.76	402 ± 16.3	Muhleman et al. (1979)
2.03	317.9 ± 1.7	This work	12.48	491.3 ± 36.9	Ulich (1974)
2.15	300 ± 20.4	Ulich (1974)	12.56	476.5 ± 11.2	Muhleman et al. (1979)
2.2	301 ± 19.4	Muhleman et al. (1979)	13.35	499.1 ± 25	Butler et al. (2001)
2.65	328.7 ± 23	Akins (2020)	13.35	505.2 ± 25.3	Butler et al. (2001)
2.98	342.7 ± 23	Akins (2020)	13.38	507 ± 22	Steffes et al. (1990)
3.17	374.5 ± 37.8	Muhleman et al. (1979)	13.4	496 ± 5.8	Perley & Butler (2013)
3.2	355.6 ± 1.3	Dahal et al. (2021)	13.41	438.8 ± 17.3	Muhleman et al. (1979)
3.41	295.9 ± 19.4	Muhleman et al. (1979)	13.41	542.9 ± 11.2	Muhleman et al. (1979)
3.48	357.5 ± 13.1	Ulich et al. (1980)	13.49	471.8 ± 31.1	Ulich (1974)
3.58	349.5 ± 32	Ulich (1974)	13.8	478.6 ± 15.3	Muhleman et al. (1979)
3.61	363.3 ± 8.2	Muhleman et al. (1979)	14.46	523.5 ± 15.3	Muhleman et al. (1979)
6.24	404 ± 19	Perley & Butler (2013)	14.59	451 ± 13.3	Muhleman et al. (1979)
6.9	405 ± 12	Perley & Butler (2013)	15.78	518.0 ± 11.5	Rubiño-Martín et al. (2023)
7.73	432.3 ± 2.8	Dahal et al. (2021)	16.03	476.5 ± 15.3	Muhleman et al. (1979)
7.99	440 ± 35	Kolodner (1997)	16.03	526.7 ± 10.9	Rubiño-Martín et al. (2023)
8.01	377.6 ± 55.1	Muhleman et al. (1979)	16.18	517.3 ± 17.3	Muhleman et al. (1979)
8.2	436 ± 13	Perley & Butler (2013)	16.24	520 ± 17	Steffes et al. (1990)
8.55	379.6 ± 35.7	Muhleman et al. (1979)	17.1	528 ± 5.8	Perley & Butler (2013)
8.72	388.8 ± 57.1	Muhleman et al. (1979)	17.63	533.1 ± 9.5	Rubiño-Martín et al. (2023)
8.88	424.5 ± 31.6	Muhleman et al. (1979)	17.95	546.6 ± 5.7	Rubiño-Martín et al. (2023)
9.08	453.6 ± 3.1	Hafez et al. (2008)	18.62	498 ± 73.5	Muhleman et al. (1979)
9.43	430.1 ± 21.4	Ulich (1974)	19.04	494.2 ± 33	Ulich (1974)
9.48	441.8 ± 20.4	Muhleman et al. (1979)	19.51	494.9 ± 48	Muhleman et al. (1979)
9.57	415.3 ± 32.7	Muhleman et al. (1979)	19.88	484.7 ± 34.7	Muhleman et al. (1979)
9.81	441.7 ± 29.1	Ulich (1974)	20	554 ± 4.7	Perley & Butler (2013)

Note. The bold values highlight the CLASS-based Venus measurements.

constraints that SO₂ is either chemically depleted within this region or inhibited from diffusive mixing (Vandaele et al. 2017). Although the exact altitude may vary within a few kilometers, the necessary SO₂ depletion altitude of the selected model aligns well with the lower middle cloud boundary (Knollenberg & Hunten 1980). A preliminary analysis from Noguchi et al. (2023) shows similar results with lower H₂SO₄ abundances from Akatsuki radio occultation measurements compared to those inferred from VEX observations used in our reference model. The temperature increase in our empirically perturbed model above the clouds is on the order of magnitude expected for diurnal and semidiurnal variability in cloud-level temperatures (Tellmann et al. 2009) and near the upper limit for lower atmospheric variability inferred from probe measurements (Seiff et al. 1985).

6. Summary

Using Jupiter as a calibration source, we measure the disk-averaged brightness temperatures of Venus at four microwave frequency bands with CLASS. In Dahal et al. (2021), we reported brightness temperatures of 432.3 ± 2.8 and 355.6 ± 1.3 K for frequency bands centered at 38.8 ± 0.5 and 93.7 ± 0.8 GHz, respectively. With the addition of a dichroic *G*-band instrument to CLASS, we measure Venus temperatures of 317.9 ± 1.7 and 294.7 ± 1.9 K at effective center frequencies of 147.9 ± 1.0 and 217.5 ± 1.0 GHz, respectively. For their respective bands, these CLASS measurements are the most precise disk-averaged Venus

brightness temperatures to date. We observe no phase dependence of the measured temperatures at all four frequency bands.

Since the wavelengths below a few centimeters are sensitive to Venusian atmospheric emission, we perform a joint analysis of the CLASS observations from ~ 1 to 8 mm and the VLA measurements from ~ 7 mm to 2 cm to obtain constraints on the accuracy of the Venus atmospheric composition models. Our analysis suggests the presence of relatively warmer mean atmospheric temperatures (i.e., by ~ 7 K) than those derived from prior radio occultation measurements. In addition, our observations indicate that the abundance of microwave absorbers inferred from the VEX radio occultation measurements could be comparatively overestimated. Further spatially resolved microwave observations of Venus could provide additional context to these disk-integrated observations.

Acknowledgments

We acknowledge the National Science Foundation Division of Astronomical Sciences for their support of CLASS under grant Nos. 0959349, 1429236, 1636634, 1654494, 2034400, and 2109311. We thank Johns Hopkins University President R. Daniels and the Kreiger School deans for their steadfast support of CLASS. We further acknowledge the very generous support of Jim and Heather Murren (JHU A&S '88), Matthew Polk (JHU A&S Physics BS '71), David Nicholson, and Michael Bloomberg (JHU Engineering '64). CLASS employs detector

technology developed in collaboration between JHU and Goddard Space Flight Center under several previous and ongoing NASA grants. Detector development work at JHU was funded by NASA cooperative agreement 80NSSC19M0005. CLASS is located in the Parque Astronómico Atacama in northern Chile under the auspices of the Agencia Nacional de Investigación y Desarrollo (ANID).



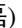
We acknowledge scientific and engineering contributions from Max Abitbol, Fletcher Boone, David Carcamo, Ted Grunberg, Saianeesh Haridas, Connor Henley, Lindsay Lowry, Nick Mehrle, Sasha Novack, Bastian Pradenas, Isu Ravi, Gary Rhodes, Daniel Swartz, Bingjie Wang, Qinan Wang, Tiffany Wei, and Ziáng Yan. We thank Miguel Angel Díaz, Jill Hanson, William Deysher, Joe Zolenas, María José Amaral, and Chantal Boisvert for logistical support. We acknowledge productive collaboration with Dean Carpenter and the JHU Physical Sciences Machine Shop team.

S.D. is supported by an appointment to the NASA Postdoctoral Program at the NASA Goddard Space Flight Center, administered by Oak Ridge Associated Universities under contract with NASA. A.A. acknowledges support from the NASA Solar System Observations program (task order 80NM0018F0612). Contributions by A.A. were carried out at the Jet Propulsion Laboratory, California Institute of Technology, under a contract with NASA (80NM0018D0004). R.R. is supported by ANID BASAL projects ACE210002 and FB210003. Z.X. is supported by the Gordon and Betty Moore Foundation through grant GBMF5215 to the Massachusetts Institute of Technology.

Software: PyEphem (Rhodes 2011), NumPy (van der Walt et al. 2011), SciPy (Virtanen et al. 2020), Astropy (Astropy Collaboration et al. 2013), Matplotlib (Hunter 2007), RadioBEAR (de Pater et al. 2014, 2019).

ORCID iDs

Sumit Dahal  <https://orcid.org/0000-0002-1708-5464>
 Alex B. Akins  <https://orcid.org/0000-0001-8379-1909>
 John W. Appel  <https://orcid.org/0000-0002-8412-630X>
 Charles L. Bennett  <https://orcid.org/0000-0001-8839-7206>
 Ricardo Bustos  <https://orcid.org/0000-0001-8468-9391>
 Joseph Cleary  <https://orcid.org/0000-0002-7271-0525>
 Jullianna D. Couto  <https://orcid.org/0000-0002-0552-3754>
 Rahul Datta  <https://orcid.org/0000-0003-3853-8757>
 Joseph Eimer  <https://orcid.org/0000-0001-6976-180X>
 Thomas Essinger-Hileman  <https://orcid.org/0000-0002-4782-3851>
 Jeffrey Iuliano  <https://orcid.org/0000-0001-7466-0317>
 Yunyang Li (李云炀)  <https://orcid.org/0000-0002-4820-1122>
 Tobias A. Marriage  <https://orcid.org/0000-0003-4496-6520>
 Carolina Núñez  <https://orcid.org/0000-0002-5247-2523>
 Matthew A. Petroff  <https://orcid.org/0000-0002-4436-4215>
 Rodrigo Reeves  <https://orcid.org/0000-0001-5704-271X>
 Karwan Rostem  <https://orcid.org/0000-0003-4189-0700>
 Rui Shi (时瑞)  <https://orcid.org/0000-0001-7458-6946>
 Deniz A. N. Valle  <https://orcid.org/0000-0003-3487-2811>
 Duncan J. Watts  <https://orcid.org/0000-0002-5437-6121>

Janet L. Weiland  <https://orcid.org/0000-0003-3017-3474>
 Edward J. Wollack  <https://orcid.org/0000-0002-7567-4451>
 Zhilei Xu (徐智磊)  <https://orcid.org/0000-0001-5112-2567>

References

- Akins, A. B., & Steffes, P. G. 2020, *Icar*, **351**, 113928
 Akins, A. B. A. 2020, PhD thesis, Georgia Tech
 Ando, H., Imamura, T., Tellmann, S., et al. 2020, *NatSR*, **10**, 3448
 Appel, J. W., Bennett, C. L., Brewer, M. K., et al. 2022, *ApJS*, **262**, 52
 Astropy Collaboration, Robitaille, T. P., Tollerud, E., et al. 2013, *A&A*, **558**, A33
 Barrett, A. H., & Staelin, D. H. 1964, *SSRv*, **3**, 109
 Bennett, C. L., Larson, D., Weiland, J. L., et al. 2013, *ApJS*, **208**, 20
 Butler, B. J., Steffes, P. G., Suleiman, S. H., Kolodner, M. A., & Jenkins, J. M. 2001, *Icar*, **154**, 226
 Dahal, S., Amiri, M., Appel, J. W., et al. 2020, *JLTP*, **199**, 289
 Dahal, S., Appel, J. W., Datta, R., et al. 2022, *ApJ*, **926**, 33
 Dahal, S., Brewer, M. K., Appel, J. W., et al. 2021, *PSJ*, **2**, 71
 Datta, R., Brewer, M. K., Couto, J. D., et al. 2022, *Proc. SPIE*, **12190**, 121902S
 de Pater, I. 1990, *ARA&A*, **28**, 347
 de Pater, I., Fletcher, L. N., Luszcz-Cook, S., et al. 2014, *Icar*, **237**, 211
 de Pater, I., Sault, R. J., Wong, M. H., et al. 2019, *Icar*, **322**, 168
 Essinger-Hileman, T., Ali, A., Amiri, M., et al. 2014, *Proc. SPIE*, **9153**, 91531H
 Fahd, A. K. 1992, PhD thesis, Georgia Tech
 Fahd, A. K., & Steffes, P. G. 1991, *JGR*, **96**, 17471
 Fahd, A. K., & Steffes, P. G. 1992, *Icar*, **97**, 200
 Fasano, A., Macías-Pérez, J. F., Benoit, A., et al. 2021, *A&A*, **656**, A116
 Fixsen, D. J. 2009, *ApJ*, **707**, 916
 Hafez, Y. A., Davies, R. D., Davis, R. J., et al. 2008, *MNRAS*, **388**, 1775
 Harrington, K., Marriage, T., Ali, A., et al. 2016, *Proc. SPIE*, **9914**, 99141K
 Hunter, J. D. 2007, *CSE*, **9**, 90
 Jenkins, J. M., Kolodner, M. A., Butler, B. J., Suleiman, S. H., & Steffes, P. G. 2002, *Icar*, **158**, 312
 Knollenberg, R. G., & Hunten, D. M. 1980, *JGR*, **85**, 8039
 Kolodner, M. A. 1997, PhD thesis, Georgia Tech
 Krasnopolsky, V. A. 2007, *Icar*, **191**, 25
 Krasnopolsky, V. A. 2012, *Icar*, **218**, 230
 Mayer, C. H., McCullough, T. P., & Sloanaker, R. M. 1958, *ApJ*, **127**, 1
 Muhleman, D. O., Orton, G. S., & Berge, G. L. 1979, *ApJ*, **234**, 733
 Nakamura, M., Imamura, T., Ishii, N., et al. 2016, *EP&S*, **68**, 75
 Noguchi, K., Onuma, H., Ando, H., Imamura, T., & Sagawa, H. 2023, in EnVision Workshop (Noordwijk: ESA)
 Orton, G. S., Antuñano, A., Fletcher, L. N., et al. 2023, *NatAs*, **7**, 190
 Oschlisniok, J., Häusler, B., Pätzold, M., et al. 2021, *Icar*, **362**, 114405
 Oyama, V. I., Carle, G. C., Woeller, F., & Pollack, J. B. 1979, *Sci*, **203**, 802
 Page, L., Barnes, C., Hinshaw, G., et al. 2003, *ApJS*, **148**, 39
 Pardo, J. R., Cernicharo, J., & Serabyn, E. 2001, *ITAP*, **49**, 1683
 Perley, R. A., & Butler, B. J. 2013, *ApJS*, **204**, 19
 Pettengill, G. H., Ford, P. G., & Wilt, R. J. 1992, *JGR*, **97**, 13091
 Planck Collaboration Int. LII 2017, *A&A*, **607**, A122
 Pollack, J. B., & Sagan, C. 1967, *ApJ*, **150**, 327
 Rhodes, C. (2011) PyEphem: Astronomical Ephemeris for Python, Astrophysics Source Code Library, ascl:1112.014
 Rubiño-Martín, J. A., Guidi, F., Génova-Santos, R. T., et al. 2023, *MNRAS*, **519**, 3383
 Seiff, A., Schofield, J., Kliore, A., et al. 1985, *AdSpR*, **5**, 3
 Steffes, P. G., Klein, M. J., & Jenkins, J. M. 1990, *Icar*, **84**, 83
 Svedhem, H., Titov, D. V., McCoy, D., et al. 2007, *P&SS*, **55**, 1636
 Tellmann, S., Pätzold, M., Häusler, B., Bird, M. K., & Tyler, G. L. 2009, *JGRE*, **114**, E00B36
 Ulich, B. 1974, *Icar*, **21**, 254
 Ulich, B., Davis, J., Rhodes, P., & Hollis, J. 1980, *ITAP*, **28**, 367
 van der Walt, S., Colbert, S. C., & Varoquaux, G. 2011, *CSE*, **13**, 22
 Vandaele, A., Korabely, O., Belyaev, D., et al. 2017, *Icar*, **295**, 16
 Virtanen, P., Gommers, R., Oliphant, T. E., et al. 2020, *NatMe*, **17**, 261
 Weiland, J. L., Odegard, N., Hill, R. S., et al. 2011, *ApJS*, **192**, 19
 Xu, Z., Brewer, M. K., Rojas, P. F., et al. 2020, *ApJ*, **891**, 134